Applied Catalysis B: Environmental 174–175 (2015) 77–84

Contents lists available at ScienceDirect

Applied Catalysis B: Environmental

journal homepage: www.elsevier.com/locate/apcatb

A novel Fe(III) porphyrin-conjugated TiO_2 visible-light photocatalyst

Binghua Yao[a,c,*], Chao Peng[a], Wen Zhang[b], Qinku Zhang[a], Jinfen Niu[a], Jie Zhao[a]

[a] Department of Applied Chemistry, Xi'an University of Technology, Xi'an 710048, China
[b] Department of Civil Engineering, University of Arkansas, Fayetteville 72701, USA
[c] The key Laboratory of Northwest Water Resources and Environmental Ecology of Ministry of Education, Xi'an University of Technology, Xi'an 710048, China

ARTICLE INFO

Article history:
Received 19 December 2014
Received in revised form 19 February 2015
Accepted 21 February 2015
Available online 23 February 2015

Keywords:
Conjugated photocatalyst
Surface modification
Sensitization
Visible-light photocatalysis
Metalloporphyrin

ABSTRACT

The metalloporphyrin tetra-carboxyphenylporphyrin iron(III) (FeTCPP) was synthesized and characterized spectroscopically. The corresponding FeTCPP-SSA/SA-TiO_2 conjugated photocatalysts were then prepared by surface chemical bonding with FeTCPP as sensitizer, 2-hydroxy-5-sulfosalicylic acid (SSA) or salicylic acid (SA) as bridging molecule, and Degussa P25 as raw material. The analysis of FT-IR and XPS spectra reveals that the specific organic complexes formed on the TiO_2 surface are linking FeTCPP molecules to TiO_2 through stable π-conjugated chemical bonds rather than physical adsorption. The morphology and structure of the as-prepared samples were characterized by UV–visible, XRD, SEM, UV–vis DRS and BET. Methylene blue (MB), as a photocatalytic degradation target, was used to evaluate the photocatalytic performance of the prepared photocatalysts. The results show that FeTCPP-SSA-TiO_2 exhibits the best photocatalytic activity among all the samples under visible light. And the new conjugated photocatalyst can be recycled 5 times, while remaining at a 90.0% MB degradation ratio.

1. Introduction

Among various semiconductor photocatalysts, TiO_2 is one of the most promising photocatalysts for the degradation of organic pollutants, due to its superior UV–photoactivity, nontoxicity and photostability [1–3]. However, the relative wide band gap (about 3.2 eV for anatase TiO_2) severely restricts its practical application [4,5]. Therefore, improving the visible photocatalytic activity of TiO_2-base photocatalysts for taking full advantage of most of the solar spectrum is an important and challenging issue. So far, most studies have been devoted to enhance the visible-light utilization of TiO_2 by doping metal ions [6–8], non-metals [9–11], semiconductor coupling [12–14], and dye sensitization [15–17]. Unfortunately, the metal/nonmetal-doped TiO_2 photocatalysts were generally rather difficult to prepare with the needs of lattice exchange at high temperature and multistep experimental process. Although semiconductor coupling could enhance the separation of photogenerated electron–hole pairs, thus increasing activity and stability, the catalytic performance strongly depends on their nano/microstructures, and energy conversion efficiencies are too low for practical applications [18,19]. The dye sensitization approach is able to dramatically extend the spectral response of TiO_2 to the visible-light region. As a dye sensitizer, the metalloporphyrin and its derivatives have attracted much attention because of their high absorption coefficient within the solar spectrum and good chemical stability compared to other dyes. Moreover, this metalloporphrin-TiO_2 system can also improve the interfacial charge transfer and lower the electron-hole recombination rate [20]. Lü [21] synthesized a series of tetraphenylporphyrin derivatives with different functional groups (—OH, $—CO_2C_2H_5$, —COOH) which were used to sensitize TiO_2, and the photocatalytic performance of TiO_2 was obviously improved. Chang [22] used nickel-porphyrin sensitized TiO_2 to degrade 2,4-dichlorophenol in wastewater under visible-light irradiation, with a maximum degradation rate reaching 81% in 240 min. Murphy [16] utilized 4-(4-carboxyphenyl) porphyrin to modify TiO_2, which efficiently degraded pharmaceutical Famotidine under visible-light irradiation. The results showed that those porphyrin or metalloporphyrin-sensitized TiO_2 catalysts all exhibit better visible-light photocatalytic performance than Degussa P25. However, most of metalloporphyrin-sensitized TiO_2, the sensitizer was only connected to the TiO_2 surface by physical/chemical adsorption instead of stable chemical bond [23,24]. So the dye molecules were easy to desorb from TiO_2 surface during the photocatalytic

* Corresponding author at: Xi'an University of Technology, Applied Chemistry, South Jinhua Road No. 5, Xi'an, China. Tel.: +86 029 82066361.
E-mail address: bhyao@xaut.edu.cn (B. Yao).

http://dx.doi.org/10.1016/j.apcatb.2015.02.030
0926-3373/

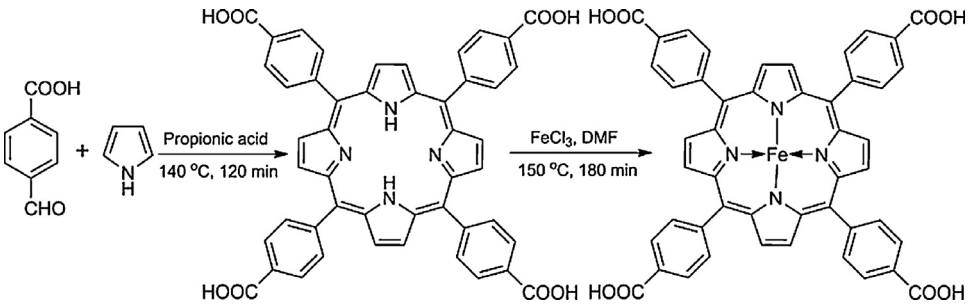

Scheme 1. Schematic illustration of the synthesis of FeTCPP complex.

reaction processes, which could decrease its photocatalytic efficiency [25,26].

The existence of anchored functional groups on the surface of TiO_2 or sensitizers is considered to be a great approach. Although metalloporphyrins containing anchoring groups could be used to sensitize TiO_2 through the formation of steady covalent bonds [27,28], their synthesis process is complicated, and time-consuming [29,30]. We consider that grafting the sensitizers on TiO_2 surface through bridging molecules is a very effective method. In our previous work, the bridging molecule tolylene-2,4-diisocyanate (TDI) was used to graft Cu-porphyrin on TiO_2 surface and the obtained photocatalyst showed potential visible photocatalytic activity and high recyclability [31]. Meanwhile, it was found out that TDI is very unstable and toxic. In this paper, a new Fe-porphyrin derivative (FeTCPP) was designed and synthesized, and then used as the sensitizer, 2-hydroxy-5-sulfosalicylic acid (SSA) or salicylic acid (SA) was used as a bridging molecule and Degussa P25 as the raw material, the novel conjugated photocatalyst FeTCPP-SSA/SA-TiO_2 was prepared. The effects of different bridging molecules on the photocatalytic activity of prepared samples were evaluated by the degradation of methylene blue (MB) under visible light irradiation.

2. Materials and methods

2.1. Reagents

All reagents were of analytical grade and were used as received without further purification except pyrrole, which was distilled before use. 2-hydroxy-5-sulfosalicylic acid (SSA) and salicylic acid (SA) were purchased from Beijing Chemical Reagent Co., Ltd.; pyrrole, carboxy benzaldehyde, and methylene blue (MB) were provided by China Sinopharm Chemical Reagent Co.; $FeCl_3$, ethanol, chloroform, methanol, and DMF were obtained from Tianjin Tianli chemical Reagent Co., Ltd. The commercial TiO_2 powder was Degussa P25 (75% anatase, 25% rutile, BET specific surface area: ~50 $m^2\ g^{-1}$, size: ~30 nm). Ultrapure deionized water was used throughout the experiments.

2.2. Synthesis of FeTCPP complex

Carboxy benzaldehyde (2.16 g) and propionic acid (150 mL) were placed into a three-necked flask, equipped with reflux condenser. The mixture was heated to 135 °C. Subsequently, a solution of pyrrole (1 mL) diluted with propionic acid (20 mL) was slowly added into the reaction solution dropwise over 60 min. The mixture solution was then refluxed for 120 min, before cooling it down to room temperature. After removing propionic acid under vacuum, the residue was dispersed in $CHCl_3$, filtered and washed with $CHCl_3$ several times. The reaction solid was then dissolved in propionic acid/$CHCl_3$ (3:2, v/v) and the insoluble impurities were removed by filtration. Finally, the crude mixture was separated by chromatography on silica gel column with propionic acid/$CHCl_3$ (3:2) as eluent. The fraction corresponding to the first colored band was collected, concentrated, and dried to give tetracarboxyphenyl-porphyrin (TCPP).

TCPP and $FeCl_3$ (molar ratio of TCPP to $FeCl_3$ was 1:1.5) were dissolved in DMF (150 mL). The mixture was heated to 150 °C using an oil bath with continuous stirring, then refluxed for 180 min. After letting the mixture cool down to room temperature, DMF was removed under vacuum. The residue was then dissolved in ethanol and the insoluble impurities were removed by filtration. Finally, the extract was concentrated and dried by rotary evaporation to yield tetracarboxyphenyl-porphyrin iron (FeTCPP). The synthetic process of FeTCPP is shown in Scheme 1.

2.3. Preparation of SSA/SA- TiO_2

TiO_2 powder (0.2 g) was dispersed in 1,4-dioxane, followed by sonication to form a homogeneous suspension. This suspension was transferred into a three-neck flask equipped with stirring, and a solution of SSA in dioxane (100 mL) was added dropwise into the flask. After refluxing for 30 min at 80 °C, the reaction mixture was filtered to obtain the SSA-TiO_2 solids. In order to remove the adsorbed and unreacted SSA, the SSA-TiO_2 solids were successively washed with dioxane, acetone, and ethanol. Finally, the solids were dried in the vacuum oven at 60 °C and the SSA-TiO_2

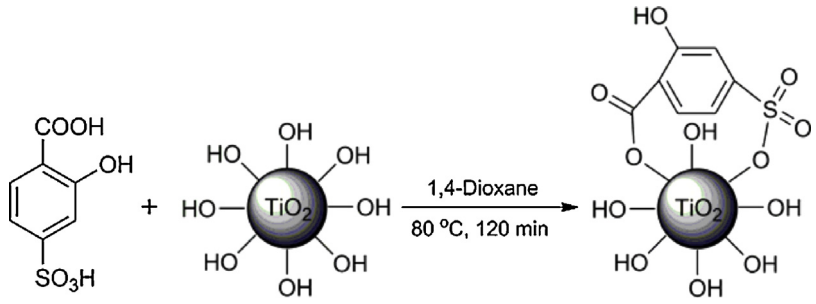

Scheme 2. Schematic illustration of the preparation of SSA-TiO_2.

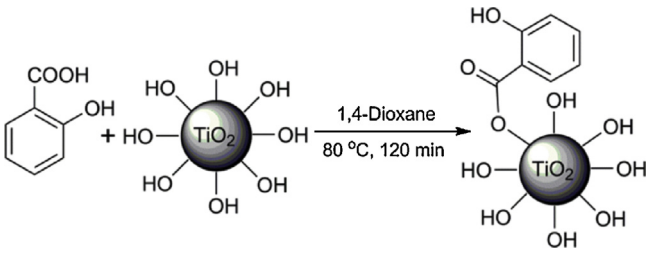

Scheme 3. Schematic illustration of the preparation of SA-TiO_2.

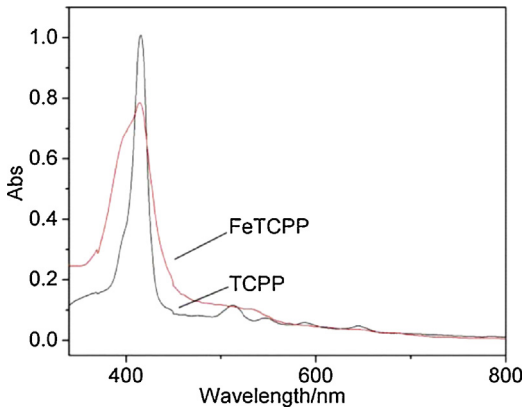

Fig. 1. UV–vis spectra of TCPP and FeTCPP.

intermediate was thus obtained. The preparation of SA-TiO_2 was similar to that of SSA-TiO_2. The preparation of SSA/SA-TiO_2 is illustrated in Schemes 2 and 3

2.4. Preparation of FeTCPP-SSA/SA-TiO_2

FeTCPP (20 mg) was dissolved in ethanol (100 mL). An appropriate amount of SSA-TiO_2 was added to the FeTCPP solution, and, after ultrasonic dispersion for 30 min, the dispersed solution was transferred into a three-necked flask. While stirring, the reaction mixture was refluxed for 120 min at 80 °C in an oil bath, then subsequently filtered. The resulting solids were washed three times with ethanol, and then dried under vacuum to obtain the FeTCPP-sensitized photocatalyst FeTCPP-SSA-TiO_2. Scheme 4 illustrates the preparation process of FeTCPP-SSA-TiO_2. The preparation of FeTCPP-SA-TiO_2 was carried out in a similar way (Scheme 5).

2.5. Preparation of FeTCPP-TiO_2

FeTCPP (20 mg) was dissolved in ethanol (100 mL). Then, an appropriate amount of TiO_2 was added to the FeTCPP solution. After ultrasonic dispersion for 30 min, the dispersed solution was transferred into a three-necked flask. While stirring, the reaction mixture was refluxed for 120 min at 80 °C in an oil bath, then the solvent was removed under vacuum. The solid residue was dried to obtain the FeTCPP-sensitized photocatalyst FeTCPP-TiO_2.

2.6. Characterization of samples

FT-IR spectrometry was conducted using a Shimadzu FT-IR 8900 (Japan), with KBr as the reference. The morphology of the samples was characterized with Hitachi S4800 and JSM-6700F (Japan), respectively. The surface properties and composition of the samples were analyzed by XPS (Thermo Fisher, ESCALAB 250Xi). The crystalline phase analysis of samples was performed via a Shimadzu XRD-7000S X-ray diffractometer (Japan) operating with a tube current of 30 mA, a tube voltage of 40 kV, and a scanning speed of 10°/min. Absorbance measurements of metalloporphyrin and its derivates were carried out using a UV-2102 PC UV–visible spectrophotometer (China). UV–vis diffuse reflectance spectra (DRS) of photocatalytic microspheres were recorded using a TU-1901 double-beam UV–vis diffuse reflectance spectrophotometer (China), with $BaSO_4$ as the reference. The N_2 adsorption–desorption isotherms of the synthesized photocatalysts were obtained by using a JW-BK122 W surface area analyzer (China).

2.7. Evaluation of visible-light catalytic activity

The photocatalytic experiment was performed using a home-made photochemical reactor, which consists of a light source, the sample tube (100 mL quartz tube: length 22.0 cm, diameter 2.0 cm, 10 cm away from the light source), a cold trap, an air bubbler, as well as several additional accessories. The source of visible light was a Xe lamp (150 W) with an emission wavelength ranging from 290 to 800 nm, and a $NaNO_2$ solution was circulated through the cooling jacket to filter out the UV emission of the lamp below 400 nm. The lamp was set inside a quartz glass condenser, which was placed inside the photochemical reactor. The temperature of the reactor was maintained at 25 °C by cooling water during the experiments. 0.05 g of photocatalysts and 50 mL of MB solution (10 mg/L) were added into tube. After air was bubbled into the reaction solution in the dark for 30 min, the light was turned on, setting the starting point ($t = 0$) of the reaction. The degradation of MB was monitored by taking an aliquot of the suspension at regular time intervals (15 min). After high-speed centrifugation of the sample, the absorbance of the supernatant was measured at 665 nm. According to the Beer–Lambert law establishing the relationship between absorbance and concentration of MB, the degradation rate η was calculated using the equation $\eta = (A_0 - A_t)/A_0 \times 100\%$. Where A_0 is the initial absorbance of the MB solution, A_t is the absorbance

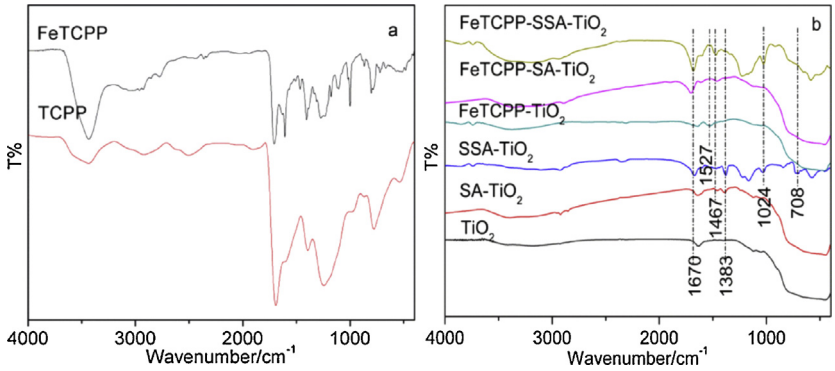

Fig. 2. FT-IR spectra of FeTCPP and TCPP (a) and the samples (b).

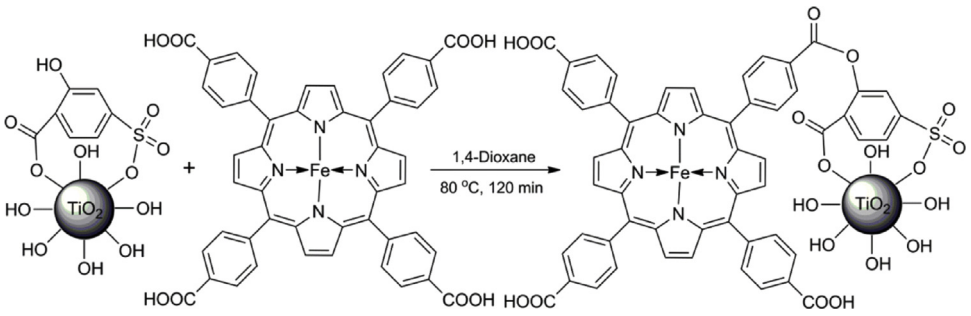

Scheme 4. Schematic illustration of the preparation of FeTCPP-SSA-TiO_2.

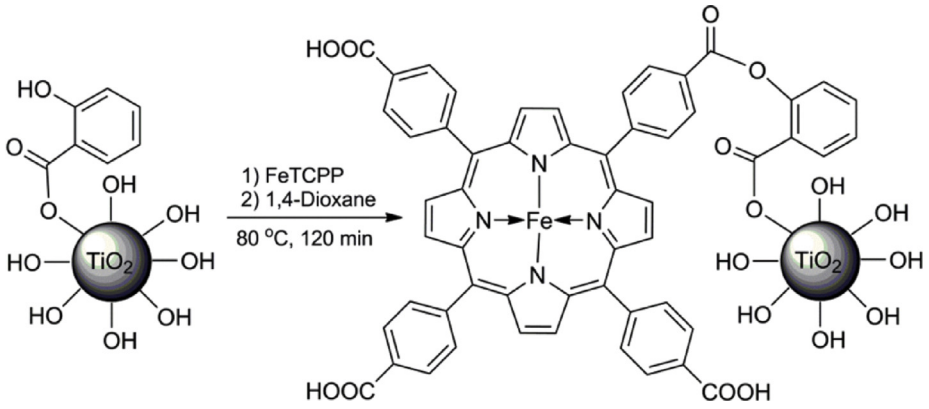

Scheme 5. Schematic illustration of the preparation of FeTCPP-SA-TiO_2.

of the MB solution at time t, and η is used to evaluate the photocatalytic activity.

3. Results and discussion

3.1. UV–vis analysis

Fig. 1 shows the UV–vis spectra of TCPP and FeTCPP. Concerning TCPP, the typical Soret band is observed at 419 nm, whereas the four weak absorption peaks in the range of 500–700 nm: 515 nm(λ_1), 550 nm(λ_2), 590 nm(λ_3) and 647 nm(λ_4) are the characteristic Q-band absorption peaks [32]. Compared to TCPP, a significant difference was observed in the spectrum of FeTCPP. Although the Soret band stays basically unchanged, only one absorption peak is still present in the Q-band, while the other peaks disappeared. Furthermore, it is noticed that the λ_1 absorption peak of FeTCPP red-shifted from 515 to 535 nm relative to TCPP, which is due to the increase in structural symmetry of the porphyrin ring when the hydrogen ions of N-H are replaced by Fe^{3+} ions [33,34].

3.2. FT-IR analysis

FT-IR analysis is a powerful tool to identify characteristic functional groups as well as the coordination between active functional groups and TiO_2. Fig. 2(a) displays the FT-IR spectra of FeTCPP and TCPP. Looking at the spectra relative to TCPP, the broad band at 3307 cm^{-1} is assigned to the stretching vibration of the N—H bonds at the center of the porphyrin ring. Compared with TCPP, the FeTCPP spectra features the characteristic stretching/bending vibration of the Fe—N bond at 1000 cm^{-1}, but the signal corresponding to N—H vibration disappeared, which demonstrates the incorporation of Fe^{3+} ion into the porphyrin ring and the formation of the metal ligand bond [35]. Fig. 2(b) shows the FT-IR spectra of different catalysts. The FT-IR spectrum of SSA-TiO_2/SA-TiO_2 displays the ester/carbonyl group peak at 1670 and 1383 cm^{-1}

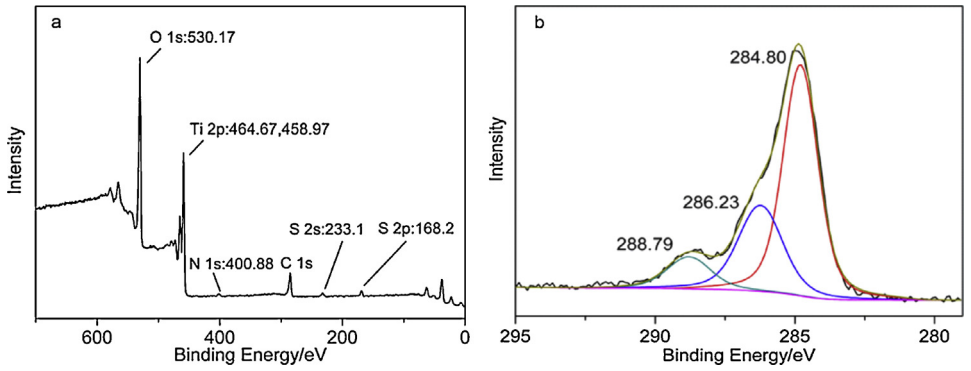

Fig. 3. XPS spectra of FeTCPP-SSA-TiO_2 (a) and its high-resolution C 1 s (b).

assigned to the —COOTi— bond, resulting from the reaction between —COOH of SSA/SA and —OH on the TiO_2 surface [36]. Furthermore, the spectrum of SSA-TiO_2 shows the characteristic absorption peak of —SO_2— at 1024 cm^{-1} relative to SSA [37]. The stretching vibration of the S=O bond is clearly observed at 708 cm^{-1} [38]. The above information indicates that the TiO_2 surface has been successfully functionalized with SSA/SA molecules. After sensitization, the spectra of both FeTCPP-SSA-TiO_2 and FeTCPP-SA-TiO_2 show an increased intensity of the peak at 1670 cm^{-1} and the bands in the region of 1225–1060 cm^{-1} attributed to the —COOC— bond resulting from the esterification between —COOH of FeTCPP and —OH of SSA/SA [39]. This reveals that the strong interaction (π-conjugated chemical bonds) between FeTCPP and SSA-TiO_2/SA-TiO_2 was established rather than simple physical adsorption. For FeTCPP-SSA-TiO_2 and FeTCPP-SA-TiO_2, the peak corresponding to the stretching vibration of the benzene ring is observed at 1467 cm^{-1}, indicating the existence of FeTCPP on the surface of modified TiO_2 (SSA/SA-TiO_2). Furthermore, this peak is obviously wider and stronger in FeTCPP-SSA-TiO_2 compared to FeTCPP-SA-TiO_2, reflecting the higher amount of FeTCPP bonded on the SSA-TiO_2 surface. This phenomenon can be attributed to the multi-functional groups of SSA, which can create stronger bridging bond-linking between FeTCPP and TiO_2. There is a slight difference between the FT-IR spectra of FeTCPP-TiO_2 and TiO_2. The low intensity peak at 1527 cm^{-1} corresponding to the benzene ring of FeTCPP further confirms the existence of FeTCPP on the surface of TiO_2. However, compared to FeTCPP-TiO_2, the peak at 1467 cm^{-1} relative to FeTCPP-SA/SA-TiO_2 shifted to longer wavelength, which can be attributed to the different interaction modes. The interaction between FeTCPP and TiO_2 in FeTCPP-SSA/SA-TiO_2 is greatly improved by the bridging units of SSA or SA through —COOTi— chemical bonds, instead of the simple physical adsorption happening in FeTCPP-TiO_2. The results displayed on FT-IR spectra are in accordance with the photocatalytic performance of the catalysts, suggesting that the π-conjugated chemical bonds between FeTCPP and TiO_2 contributes to the improvement of the photocatalytic activity.

3.3. XPS analysis

The X-ray photoelectron spectra (XPS) of FeTCPP-SSA-TiO_2 and its high-resolution C (1s) are shown in Fig. 3. In Fig. 3(a), the peaks located at 168.2 eV and 233.1 eV can be attributed to the S (2s) and S (2p) in the —SO_2—O— unit, and the weak peak at 400.88 eV is ascribed to the N (1s) in FeTCPP. The C (1s) signals at 284.80, 286.23 and 288.79 eV as shown in Fig. 3(b) are ascribed to FeTCPP or SAA units. This indicated that the FeTCPP and SSA were well bonded on the surface of TiO_2. In addition, from the XPS analysis of O (1s) and Ti (2p) of FeTCPP-SSA-TiO_2 (Fig. 3a), it was found that

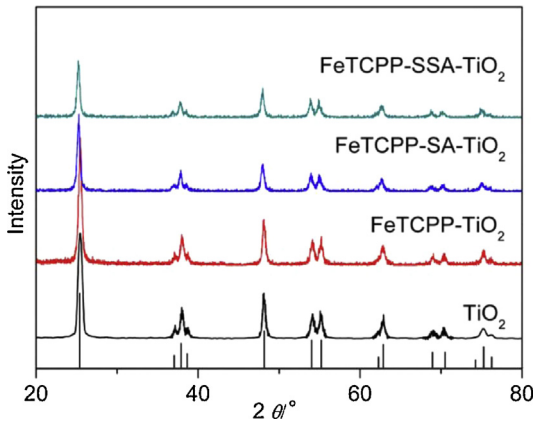

Fig. 4. XRD patterns of the samples.

the slight shifts to lower binding energy for O (1s, 530.17 eV) and Ti (2p, 458.97, 464.67 eV) compared to the reported binding energy of the bare TiO_2 (531.01 eV for O (1s), and 460.06, 465.80 eV for Ti (2p) [21], which was probably due to the weak interactions between SSA molecules and TiO_2. Moreover, from the XPS analysis of C (1s) in Fig. 3(b), the slight lower binding energy shifts of the three peaks for C (1s) by comparison with those in the literature data (286.4, 289.3 and 290.0 eV) [40] further confirmed that the FeTCPP-SSA well impregnated onto the surface of the TiO_2.

3.4. XRD analysis

The crystalline phases of the catalysts were characterized by XRD. As shown in Fig. 4, all the diffraction peaks can be assigned to the anatase structure of TiO_2 (JCPDS No. 21-1272) [41]. The characteristic diffraction peaks of FeTCPP-TiO_2, FeTCPP-SSA-TiO_2 and FeTCPP-SA-TiO_2 in XRD patterns do not exhibit any shifts or any changes in peak shape, which indicates that the modification and sensitization has no influence on the crystal structure of TiO_2.

3.5. SEM analysis

The SEM images of TiO_2 and FeTCPP-SSA-TiO_2 are shown in Fig. 5. As shown in Fig. 5(a), TiO_2 particles display uniform spherical shape and smooth surface with an average diameter of 40 nm. The morphology of FeTCPP-SSA-TiO_2 (Fig. 5(b)) is characterized by the presence of irregular spheres with loose and rough surface, with an average diameter of about 100 nm for these microspheres. This phenomenon is due to the formation of the organic shell (FeTCPP-SSA), generated from the reaction between FeTCPP and SSA molecules

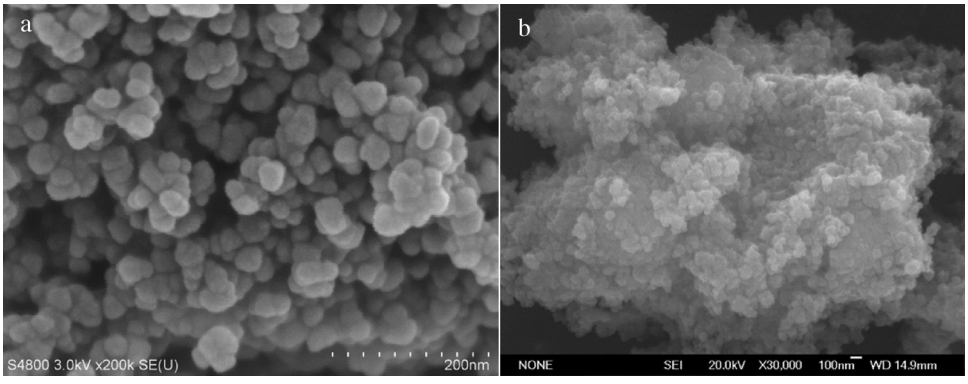

Fig. 5. SEM micrographs of bare TiO_2 (a) and FeTCPP-SSA-TiO_2 (b).

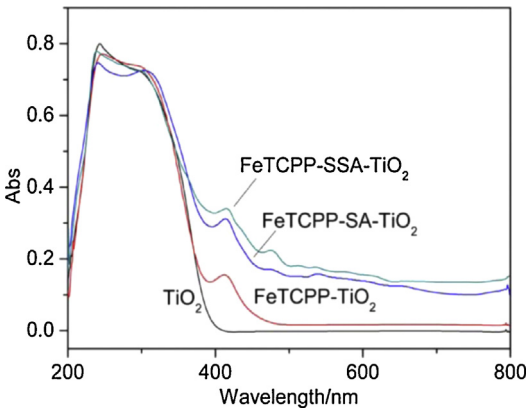

Fig. 6. UV–vis-DRS spectra of bare TiO_2 and the samples.

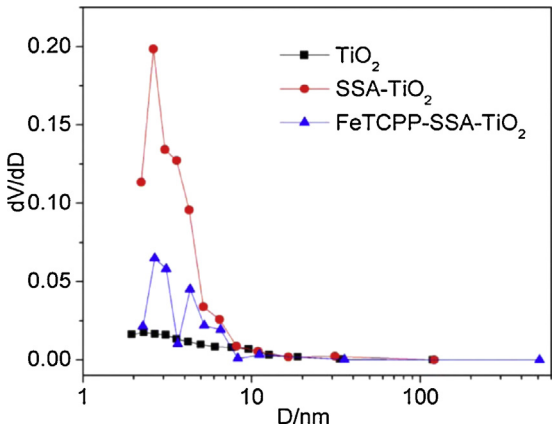

Fig. 8. Pore size distribution of bare TiO_2, SSA-TiO_2 and FeTCPP-SSA-TiO_2, determined from corresponding adsorption–desorption isotherms.

on the surface of the TiO_2 particles. Simultaneously, this surface modification resulted in the aggregation of FeTCPP-SSA-TiO_2. This implies that TiO_2 particles were all coated with the organic shell of FeTCPP and SSA molecules. The organic shell is a substrate compatible with MB molecules, thus enhancing adsorption of MB and promoting sensitizer efficiency.

3.6. UV–vis DRS analysis

In order to study the optical response of the samples, the UV–vis DRS absorption spectra of were measured as shown in Fig. 6. It was found that there was no absorption above 400 nm for bare TiO_2. However, all of the FeTCPP-SSA-TiO_2, FeTCPP-SA-TiO_2 and FeTCPP-TiO_2 exhibited the characteristic peak of FeTCPP at 419 nm (Soret band). It is worth noting that it was higher for FeTCPP-SSA-TiO_2 or FeTCPP-SA-TiO_2 photocatalyst than that of the FeTCPP-TiO_2, which further confirms the existence of the strong interaction between FeTCPP and SSA/SA-TiO_2 via chemical bridging bond-linking with maintaining the porphyrin unit. These data lead to the preliminary conclusion that FeTCPP successfully bonded onto the surface of SSA/SA-TiO_2. In addition, a considerable increase in absorbance in the range of 500–800 nm is also observed for FeTCPP-SSA/SA-TiO_2. This indicates that the occurrence of electronic interactions between SSA/SA and TiO_2, as well as the visible light response of 500–800 nm can be attributed to the formation of "—COOTi—" on the TiO_2 surface [42], which led to the light yellow color of the FeTCPP-SSA/SA-TiO_2 powder [35]. This conclusion is consistent with that the results of FT-IR spectra.

3.7. BET analysis

The N_2 adsorption–desorption isotherms of TiO_2, SSA-TiO_2 and FeTCPP-SSA-TiO_2 are displayed in Fig. 7. According to the IUPAC classification, TiO_2 exhibits type III pattern with H4-type hysteresis loop, while SSA-TiO_2 and FeTCPP-SSA-TiO_2 exhibit typical type IV patterns with H3-type hysteresis loop, which is characteristic of mesoporous materials [23]. Looking at the hysteresis loop of SSA-TiO_2, a sharp increase in the adsorption curve at high relative pressure (P/P_0) of 0.3–0.9 is the result of the capillary condensation of N_2 molecules inside the mesopores, which implies the existence of uniform mesopores formed by the organic shell of SSA on the surface of TiO_2. The specific surface area of SSA-TiO_2 is 92.4 $m^2\,g^{-1}$, which is significantly larger than those of TiO_2 (46.4 $m^2 \cdot g^{-1}$) and FeTCPP-SSA-TiO_2 (62.6 $m^2 \cdot g^{-1}$). The corresponding pore size distributions are presented in Fig. 8. Mesopores (from 2 to 8 nm) are mainly observed on both SSA-TiO_2 and FeTCPP-SSA-TiO_2, which implies a uniform quality for these mesoporous catalysts with an average pore size of 21.2 nm and 18.1 nm respectively. The results suggest that the introduction of SSA led to a significant increase in the specific surface area and average pore size, which are more favorable for adsorption and further degradation of organic pollutants, and can provide more active sites for the photocatalytic reaction.

3.8. Evaluation of photocatalytic activity

The photocatalytic activity of the samples was evaluated by measuring the degradation of MB under visible-light irradiation. Fig. 9 shows the efficiency of different catalysts for MB

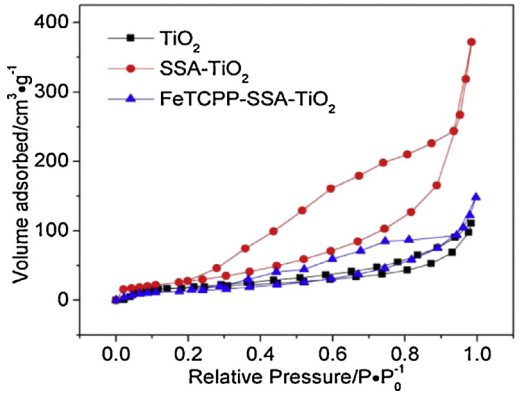

Fig. 7. Nitrogen adsorption–desorption isotherms of bare TiO_2, SSA-TiO_2 and FeTCPP-SSA-TiO_2.

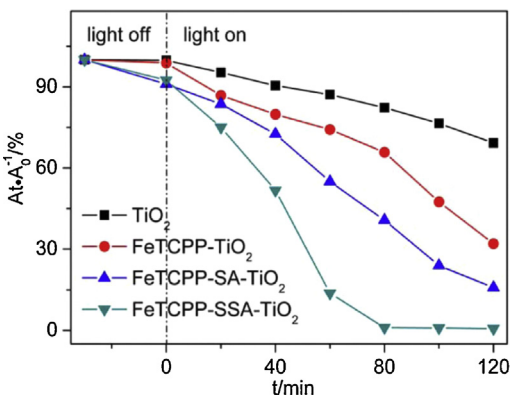

Fig. 9. Photocatalytic performance of the samples for the degradation of MB.

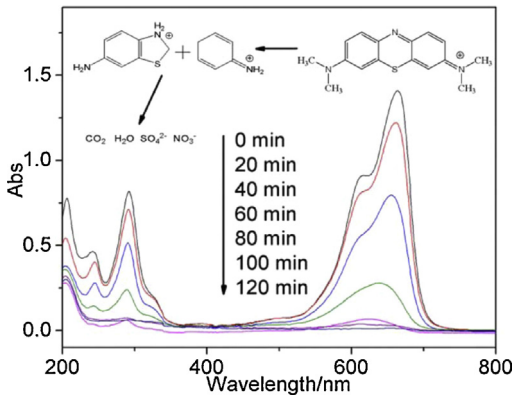

Fig. 10. UV–vis absorption curves of the photocatalytic degradation of MB over FeTCPP-SSA-TiO_2 under Xe lamp irradiation.

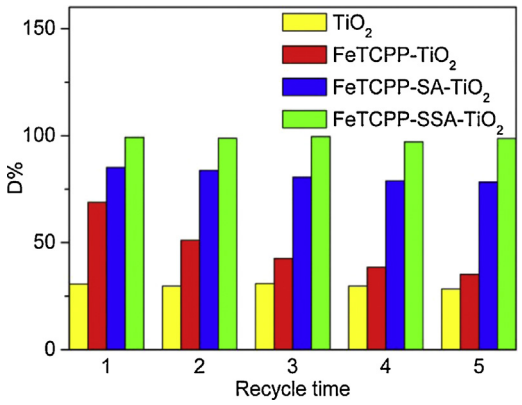

Fig. 11. Photocatalytic degradation rate of the samples for MB in five cycles.

photocatalytic degradation. It is clearly observed that, during the adsorption–desorption equilibrium process, FeTCPP-SSA-TiO_2 and FeTCPP-SA-TiO_2 exhibit a larger capacity to absorb MB compared to TiO_2, which can be attributed to the excellent adsorption properties of FeTCPP-SSA/SA complexes. Under Xe lamp irradiation, it is worth noting that FeTCPP-SSA-TiO_2 shows the best photocatalytic activity for the degradation of MB with a degradation rate of 99.3% within 120 min. It is significantly higher than that of FeTCPP-SA-TiO_2 (85.2%), FeTCPP-TiO_2 (68.9%), and TiO_2 (30.7%). Fig. 10 displays the changes observed in the absorbance of MB in aqueous solution exposed to visible light at different time intervals in the presence of FeTCPP-SSA-TiO_2. The inset describes the degradation pathway of MB. As shown, the characteristic absorption band around 665 nm can be attributed to a chromophore containing a long conjugated π system, while the absorption peaks at 245 and 292 nm are related to aromatic rings [24]. According to Fig. 10, the disappearance of the 664 nm absorption band suggests that the conjugated π bond of the molecular structure of MB was broken [25]. The decrease in intensity of the absorption bands around 245 and 290 nm in the UV region is due to the breaking of the aromatic rings in the MB molecules which confirms the destruction of degradation intermediates including aminobenzothiazole and aniline [25,43]. All of these data indicates that MB molecules were completely degraded to inorganic molecules (CO_2, H_2O, SO_4^{2-}, NO_3^-) [24,26] by the FeTCPP-SSA-TiO_2 photocatalysts under visible light irradiation. The surface modification with SSA optimized the surface properties of TiO_2 and strengthened the adhesion strength of sensitizers. The bridging bond-linking units effectively inhibited the detachment of FeTCPP from the surface of modified TiO_2 during the photocatalytic process. And the stronger adhesion strength between FeTCPP and SSA-TiO_2 not only increases the amount of FeTCPP adhering to the surface of SSA-TiO_2, but also facilitates electron transfer from excited FeTCPP molecules to the conduction band of TiO_2 [20]. Thus, the FeTCPP-SSA-TiO_2 exhibits the highest photocatalytic activity for the degradation of MB under visible light.

In order to investigate the long-term stability of FeTCPP-SSA-TiO_2 and FeTCPP-SA-TiO_2, the photocatalysts were recycled after each photocatalytic degradation experiment, and then were reused in the next run. As shown in Fig. 11, the FeTCPP-SSA-TiO_2 photocatalysts can efficiently degrade MB under visible light without significant deactivation after 5 cycles (degradation efficiency remains about 90%). As compared with FeTCPP-SSA-TiO_2, the degradation efficiency of MB in the presence of FeTCPP-TiO_2 decreases rapidly after recycling, which can be due to FeTCPP coming apart from the TiO_2 surface. The weak bridging bond-linking (SA molecules possess less functional groups than SSA molecules) leads to a slower decrease of the degradation efficiency for FeTCPP-SA-TiO_2. These results demonstrate that SSA can form a steady chemical bridging bond-linking between FeTCPP and TiO_2, thus enhancing the photocatalytic performance, stability and recyclability of FeTCPP-SSA-TiO_2.

4. Conclusion

In summary, the main goal of the present study was to obtain the new conjugated photocatalysts FeTCPP-SSA/SA-TiO_2, which were achieved by chemically linking the sensitizer through a combination of the FeTCPP sensitization and the surface modification technique. The characterizations of the morphology and structure of FeTCPP-SSA/SA-TiO_2 indicate that the bridging bond-linking interaction occurs between SSA/SA-TiO_2 and FeTCPP with SSA/SA molecules as bridging bond-linking units. What's more, SSA plays a crucial role in immobilizing firmly FeTCPP on the surface of TiO_2. The significant improvement of the photocatalytic activity and successful inhibition of the detachment of the sensitizer are mainly attributed to the multi-functional groups of SSA. FeTCPP-SSA-TiO_2 possesses an excellent efficiency toward the degradation of MB (99.3%) under visible light irradiation, long-term stability and reusability, up to 5 times without significant deactivation. All of these unique properties suggest that FeTCPP-SSA-TiO_2 conjugated microspheres have a bright future, especially applied to waste water treatment.

Acknowledgements

This work was supported by the National Natural Science Foundation of China (No. 21276208), the Doctor Foundation of Education Ministry of China (No. 20096118110008), the Special Research Fund of Shaanxi Provincial Department of Education of China (No. 12JK0606), and the Research Fund for Excellent Doctoral Thesis of Xi'an University of Technology (No. 207-002J1304).

References

[1] K. Nakata, A. Fujishima, J. Photochem. Photobio. C: Photochem. Rev. 13 (2012) 169–189.
[2] R. Dholam, N. Patel, A. Santini, A. Miotello, Int. J. Hydrogen Energy 35 (2010) 9581–9590.
[3] A.O. Kondrakov, A.N. Ignatev, F.H. Frimmel, S. Bräse, H. Horn, A.I. Revelsky, Appl. Catal. B: Environ. 160–161 (2014) 106–114.
[4] N. De la Cruz, R.F. Dantas, J. Giménez, S. Esplugas, Appl. Catal. B: Environ. 130–131 (2013) 249–256.
[5] R. Ramakrishnan, S. Kalaivani, J.A.I. Joice, T. Sivakumar, Appl. Surf. Sci. 258 (2012) 2515–2521.
[6] X.F. Lei, X.X. Xue, H. Yang, Appl. Surf. Sci. 321 (2014) 396–403.
[7] S.C. Xu, S.S. Pan, Y. Xu, Y.Y. Luo, Y.X. Zhang, G.H. Li, J. Hazard. Mater. 283 (2015) 7–13.
[8] A.H. Gordillo, V.R. González, Chem. Eng. J. 261 (2015) 53–59.
[9] M.J. Powell, R.G. Palgrave, C.W. Dunnill, I.P. Parkin, Thin Solid Films 562 (2014) 223–228.

[10] M.J. Mattle, K.R. Thampi, Appl. Catal. B: Environ. 140–141 (2013) 348–355.
[11] V.M. Menendez-Flores, D.W. Bahnemann, T. Ohno, Appl. Catal. B: Environ. 103 (2011) 99–108.
[12] D.N. Liu, G.H. He, L. Zhu, W.Y. Zhou, Y.H. Xu, Appl. Surf. Sci. 258 (2012) 8055–8060.
[13] B.M. Almeida, M.A. Melo Jr., J. Bettini, J.E. Benedetti, A.F. Nogueira, Appl. Surf. Sci. 324 (2015) 419–431.
[14] S.B. Rawal, D.P. Ojha, S.D. Sung, W.I. Lee, Catal. Commun. 56 (2014) 55–59.
[15] C.A. Páez, S.D. Lambert, D. Poelman, J.P. Pirard, B. Heinrichs, Appl. Catal. B: Environ. 106 (2011) 220–227.
[16] S. Murphy, C. Saurel, A. Morrissey, J. Tobin, M. Oelgemöller, K. Nolan, Appl. Catal. B: Environ. 119–120 (2012) 156–165.
[17] S. Ananthakumar, J. Ramkumar, S.M. Babu, Solar Energy 106 (2014) 136–142.
[18] P. Heremans, D. Cheyns, B.P. Rand, Acc. Chem. Res. 42 (2009) 1740–1747.
[19] J. Zhang, Q. Xu, Z.C. Feng, M.J. Li, C. Li, Angew Chem. Int. Ed. 47 (2008) 1766–1769.
[20] G. Mele, R.D. Sole, G. Vasapollo, G. Marc, E. Garcia-Lopez, L. Palmisano, J.M. Coronado, M.D.H. Alonso, C. Malitesta, M.R. Gualcito, J. Phys. Chem. B 109 (2005) 12347–12352.
[21] X.F. Lü, W.J. Sun, J. Li, W.X. Xu, F.X. Zhang, Spectrochim. Acta. Part A 111 (2013) 161–168.
[22] M.Y. Chang, Y.H. Hsieh, T.C. Cheng, K.S. Yao, M.C. Wei, C.Y. Chang, Thin Solid Films 517 (2009) 3888–3891.
[23] K.S.W. Sing, D.H. Everett, R.A.W. Haul, L. Moscou, R.A. Pierotti, J. Rouquerol, T. Siemieniewska, Pure Appl. Chem. 57 (1985) 603–619.
[24] T. Soltani, M.H. Entezari, J. Mol. Catal. A: Chem. 377 (2013) 197–203.
[25] A. Houas, H. Lachheb, M. Ksibi, E. Elaloui, C. Guillard, J.M. Herrmann, Appl. Catal. B: Environ. 31 (2001) 145–157.
[26] F.X. Shao, L.Y. Zhou, F.Y. Zhang, B.Y. Wen, Y.Y. Wen, J.L. Jin, Z. Fan, Ultrason. Sonochem. 19 (2012) 756–761.
[27] G.G. Oliveros, E.A.P. Mozo, F.M. Ortega, M.T. Piccinato, F.N. Silva, C.L.B. Guedes, E.D. Mauro, M.F. da Costa, A.T. Ota, J. Mol. Catal. A: Chem. 339 (2011) 79–85.
[28] L.G. Devi, M.L.A. Kumari, Appl. Surf. Sci. 276 (2013) 521–528.
[29] C.J.P. Monteiro, M.M. Pereira, M.G.H. Vicente, L.G. Arnaut, Tetrahedron 68 (2012) 8783–8788.
[30] B.J. Gao, L. Fang, J.Y. Men, Q.J. Lei, Mater. Chem. Phys. 134 (2012) 1049–1058.
[31] C. Peng, B.H. Yao, W. Zhang, J.F. Niu, J. Zhao, Chin. J. Chem. Phys. 27 (2014) 200–208.
[32] R. Buntem, A. Intasiri, W. Lueangchaichaweng, J. Colloid Interface Sci. 347 (2010) 8–14.
[33] Y. Kitamura, M. Mifune, D. Hino, S. Yokotani, M. Saito, I. Tsukamoto, A. Iwado, Y. Saito, Talanta 69 (2006) 43–47.
[34] S. Zakavi, S. Talebzadeh, S. Rayati, Polyhedron 31 (2012) 368–372.
[35] S.X. Li, F.Y. Zheng, W.L. Cai, A.Q. Han, Y.K. Xie, J. Hazard. Mater. B 135 (2006) 431–436.
[36] F.M. Arkaitz, B. Gotzone, B. Begoña, M.K. Urtiaga, M.I. Arriortua, Polyhedron 30 (2011) 2711–2716.
[37] Y. Sun, Y. Wang, I. Zhitomirsky, Colloids Surf. A 418 (2013) 131–138.
[38] H.X. Guo, K.L. Lin, Z.S. Zheng, F.B. Xiao, S.X. Li, Dyes Pigm. 92 (2012) 1278–1284.
[39] Q.L. Tan, X.J. Zhang, L.J. Mao, G.Q. Xin, S.F. Zhang, J. Mol. Struct. 1035 (2013) 400–406.
[40] X. Wang, H.M. Zhao, X. Quan, Y.Z. Zhao, S. Chen, J. Hazard. Mater. 166 (2009) 547–552.
[41] S.X. Li, S.J. Cai, F.Y. Zheng, Dyes Pigm. 95 (2012) 188–193.
[42] H.L. Liu, Y. Zhou, H.Y. Huang, Y.Y. Feng, Desalination 278 (2011) 434–437.
[43] Q. Wang, S.L. Tian, J. Long, P. Ning, Catal. Today 224 (2014) 41–48.